Scanning Electron Microscopy

Volume 1986
Number 3 *Part III*

Article 1

7-28-1986

Ion Optics of Submicron Ion Beams

H. Liebl
Max-Planck-Institut für Plasmaphysik

H. Weiss
Max-Planck-Institut für Plasmaphysik

SCANNING ELECTRON MICROSCOPY/1986/III (Pages 793-798)
SEM Inc., AMF O'Hare (Chicago), IL 60666-0507 USA

0586-5581/86$1.00+05

ION OPTICS OF SUBMICRON ION BEAMS

H. Liebl* and H. Weiss

Max-Planck-Institut für Plasmaphysik
EURATOM Association, D-8046 Garching/München, F.R.G.

(Received for publication May 05, 1986, and in revised form July 28, 1986)

Abstract

An electrostatic objective lens for focusing ion beams to very small diameters on a plane, conducting sample surface was designed. The lens can focus ions of either polarity in the decel-accel or accel-decel mode and collect and collimate secondary charged particles of either polarity emitted with low initial energy. Moreover, a microscopic mirror objective for visual observation of the sample surface in situ is incorporated in the electrostatic optics.

KEY WORDS: Ion optics, ion microprobes, image aberrations, secondary ion mass spectrometry.

*Address for correspondence:
H. Liebl
Max-Planck-Institut für Plasmaphysik
D-8046 Garching
W. Germany Phone No. (089) 3299 249

Introduction

In an ion beam column for generating microbeams, one of the basic problems is to focus a sufficient beam intensity into the tiny spot. In cases where the microspot is formed by strong demagnification of the virtual source or a physical aperture (Köhler illumination), the beam current focused in the spot is given by the expression /10, 8/:

$$I_B = \beta \left(\frac{d_g}{2} \pi \frac{r_a}{b}\right)^2 , \qquad (1)$$

where β (A cm^{-2} sr^{-1}) is the ion gun brightness or the brightness prevailing at the Köhler aperture, d_g the geometric spot diameter, r_a the beam aperture radius at the objective lens, and b the image distance of the spot from the lens. Given a certain brightness and spot diameter d_g, eq. (1) shows that the probe current I_B increases with $1/b^2$ when the working distance is shortened.

The other way of increasing the probe current would be to increase the beam aperture r_a. But this can only be done up to a point where one of the r_a-dependent image aberrations becomes comparable with the geometric spot size d_g. These are the spherical aberrations /9/:

$$d_s = \frac{K_s}{D^2} r_a^3 , \qquad (2)$$

where K_s is a dimensionless lens-specific factor ranging from 2 to 10 for einzel lenses and D is a scaling parameter (in cm) related to the axial extent of the lens field, and the chromatic aberration

$$d_c = K_c \frac{\Delta V}{V} r_a , \qquad (3)$$

where K_c is a dimensionless factor ranging from 1 to 5 for einzel lenses, and $\Delta V/V$ is the relative energy spread of the ions.

Since the aberrations (in first approximation) do not depend on the image distance b, it is easy to see that it really helps to make b as short as possible.

In cases where the spot is formed as an image of a field ion source (liquid metal sources included), d_g becomes negligibly small so that another expression replaces eq. (1):

$$I_B = \frac{dI}{d\Omega}\,\pi\,(M\,\frac{r_a}{b})^2 \quad , \qquad (4)$$

where $dI/d\Omega$ is the angular intensity of the source and M the imaging ratio from source to sample. Whereas in the previous case $M \ll 1$, in this case M is typically of the order of unity /6/. Since M (see /8/, eq. (13)) is proportional to b, the latter cancels out of eq. (4). But on the other hand, here the aberrations due to the first condenser lens contribute to the spot diameter, too, because M is not small. They are transferred from source to sample with some power of M, so that their contribution increases with b. The conclusion is that in this case, too, it is advantageous to make b as short as possible.

This implies that the sample surface should be placed at the very exit of the objective lens. In many applications of microbeams, particularly the ones we are concerned with, i.e., secondary-ion mass spectrometry (SIMS), a signal of secondary charged particles must be collected. In SIMS it is the secondary ions, in scanning ion microscopy (SIM) it is the secondary electrons. The best way to do this, then, is to extract them backwards through the lens and separate them afterwards from the primary beam. This principle has already been successfully applied in a SIMS apparatus in the authors' laboratory /3, 4, 1/, but only for secondary ions of charge polarity opposite to that of the primary beam. At present we are operating with primary Cs^+ ions and collecting the negative secondary ions for mass analysis. In order to collect the positive secondary ions, we would have to use negative primary ions. These are more difficult to produce with acceptable brightness. We therefore wanted an objective lens which could be generally applied for primary and secondary charged particles of opposite or equal charge polarity. This would be advantageous for SIMS applications, allowing us to use also primary O_2^+ ions and positive secondary ions. Working with field ion sources which produce positive ions, one could then utilize the secondary electrons for SIM, or the positive secondary ions for SIMS.

Analytical approach

In a first approach we considered an arrangement of thin, plane apertured electrodes B_i (Fig. 1) arranged coaxially on the normal of a conducting, plane surface with the distances d_i and kept at the potentials V_i against the sample potential /7/. The axial potential distribution of such an arrangement is composed of straight sections and kinks. The trajectories of charged particles through the straight sections (uniform fields) are pieces of parabolas, and the kinks act as lenses (Davisson-Calbick approximation /2/). The transfer matrix method was applied. Primary ions enter the assembly through aperture B_n at a distance r_{np} from the axis including the angle r'_{np} with the axis. They have the energy e $(V_p + V_n)$; the positive sign applies when primaries and secondaries have equal charge polarity, the negative sign for opposite charge polarity. They arrive at the sample at a

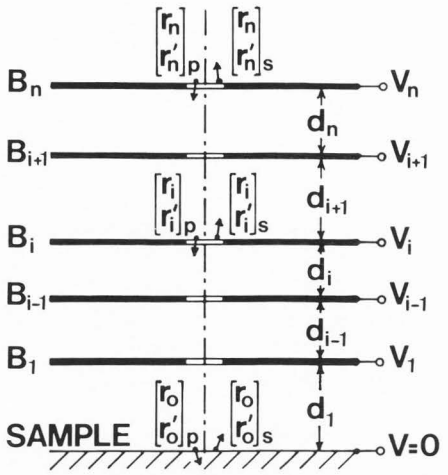

Fig. 1: Electrode assembly generating an axial potential distribution composed of straight sections and kinks. Primary charged particles enter the assembly at radial distance r_{np} from axis with angle r'_{np} and energy e $(V_p + V_n)$, secondary charged particles leave the sample surface at radial distance r_{os} from axis with angle r'_{os} and initial energy eV_o $(V_o \ll V_i)$

distance r_{op} from the axis with the angle r'_{op} to it. In matrix form this is written as:

$$\begin{bmatrix} r_o \\ r'_o \end{bmatrix}_p = \begin{bmatrix} p_{11} & p_{12} \\ p_{21} & p_{22} \end{bmatrix} \begin{bmatrix} r_n \\ r'_n \end{bmatrix}_p . \qquad (5)$$

The transfer matrix with the coefficients p_{ik} is found as the matrix product of all single transfer matrices of the apertures B_i and distances d_i.

A parallel paraxial primary pencil is focused on the sample when $p_{11} = 0$. The focal length of the objective lens thus defined is $f_p = -1/p_{21}$.

Likewise, we let a secondary charged particle start from the sample with low initial energy eV_o $(V_o \ll V_i)$ at a distance r_{os} from the axis with an angle r'_{os}. It leaves the aperture B_n at a distance r_{ns} with an angle r'_{ns}. This is written as:

$$\begin{bmatrix} r_n \\ r'_n \end{bmatrix}_s = \begin{bmatrix} s_{11} & s_{12} \\ s_{21} & s_{22} \end{bmatrix} \begin{bmatrix} r_o \\ r'_o \end{bmatrix}_s . \qquad (6)$$

The transfer matrix with the coefficients s_{ik} is again found as the matrix product of all single transfer matrices.

Secondaries emitted into the half-space with low initial energy from a surface point leave the last aperture B_η as a parallel pencil when $s_{22} = 0$.

Solutions are cases where both conditions $p_{11} = 0$ and $s_{22} = 0$ are simultaneously met. Then the electrode array acts as objective lens for the primary beam and at the same time as emission lens for the secondary charged particles.

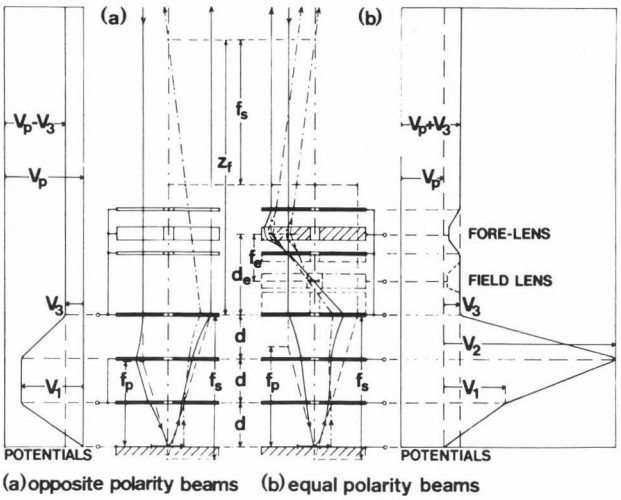

Fig. 2: Combined objective and emission lens switchable for beams of opposite (a) or equal (b) charge polarity. Conditions for mode (a): $V_p = 4.5\ V_3$, $V_1 = V_2 = 3.55\ V_3$, $f_p = 1.9\ d$, $f_s = 3.3\ d$; einzel lens not activated. Conditions for mode (b): $V_p = 2.5\ V_3$, $V_1 = 3.55\ V_3$, $V_2 = 10\ V_3$, $f_p = 2.26\ d$; einzel lens activated, $d_e = 1.83\ d$, $f_e = 1.07\ d$, $f_s = 3.3\ d$. The example is chosen such that in both modes the primary beam entrance energy is the same, viz., $e(V_p \pm V_3) = 3.5\ V_3$, that the field strength at the surface is the same, viz., $3.55\ V_3/d$ and that f_s is the same. By activating a field lens (dashed) placed at the intermediate image, the overall backfocal plane can be made to occur at the same position as with mode (a). The effect of the two einzel lenses on the primary beam is very weak because of its much higher energy

Numerical analysis shows that in the case of opposite charge polarity solutions are possible with only two electrodes. This had already been found /5/. The primaries are then focused in a decel-accel field, which acts on the secondaries as an accel-decel field.

In the case of equal charge polarity, however, where the primaries must be focused with an accel-decel field, this focusing field acts on the secondaries as such a strong lens that they experience a crossover shortly after passing it and form a diverging pencil afterwards. Three more electrodes must therefore be added acting as an einzel lens upon the secondary beam and making it parallel.

Figure 2 shows an example of a solution where both cases can be covered with the same set of electrodes by switching the potentials applied to them.

The separation of the two beams afterwards poses no problem since they have very different energies. From Fig. 2 it is evident that the primary beam energy is much higher than the secondary beam energy. An electrostatic deflector can be employed for that.

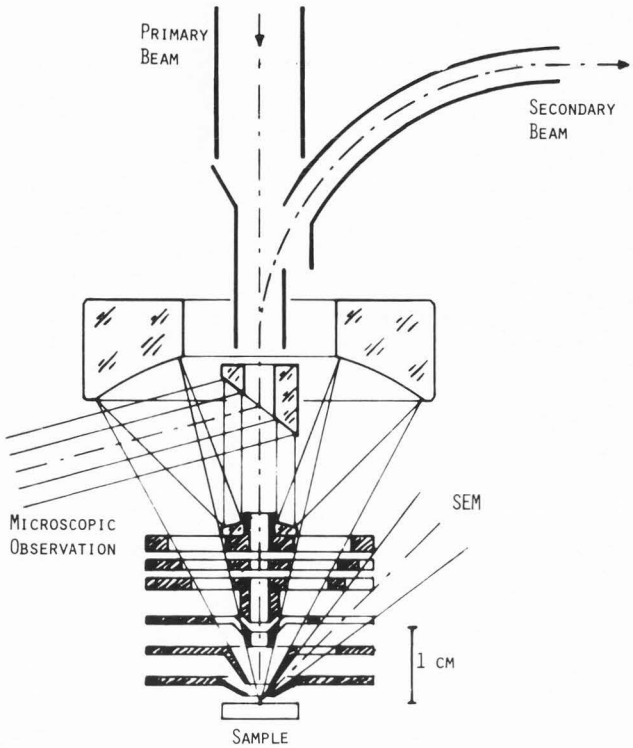

Fig. 3: Combined electrostatic objective and emission lens with light microscope

The actual lens design

The analytical approach provided a good basis for the actual lens design, especially as to the axial potential distribution required to obtain the ion optical properties outlined above.

But a set of electrodes with small apertures is not a practical solution, mainly with regard to off-axis scanning of the beams and image aberrations. Moreover, the actual design had to take into account other desired features such as the incorporation of a light-optical mirror objective for microscopic viewing of the sample in situ. This feature has proved itself as extremely valuable in previous designs.

Figure 3 shows an outline of the new design. The mirror objective (Schwarzschild or Cassegrain type) necessitates conical shapes of the electrodes generating the main field to allow passage of the light to and from the sample surface. This has a beneficial side effect: The bombarded spot "sees" only the narrow edges of the electrodes near to it, thereby minimizing background signals and memory effects due to particles reflected and material sputtered from them. The main field is generated by three electrodes followed by three more electrodes forming an einzel lens.

In order to verify the expected ion optical properties and find the electrode potentials required, computer ray tracing was performed. Solutions were found by trial and error.

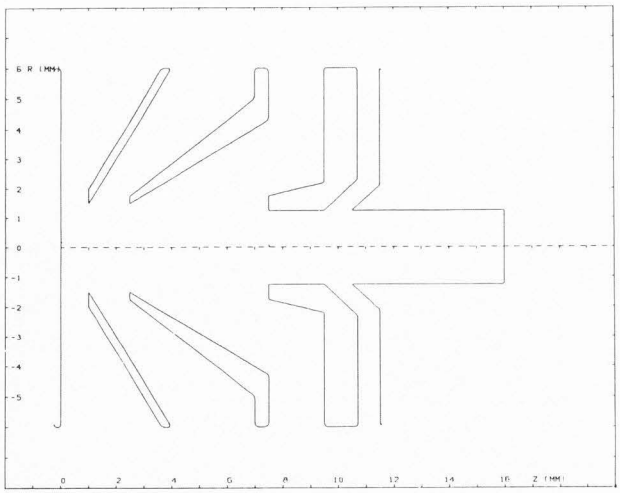

Fig. 4: Electrode geometry of the new objective lens

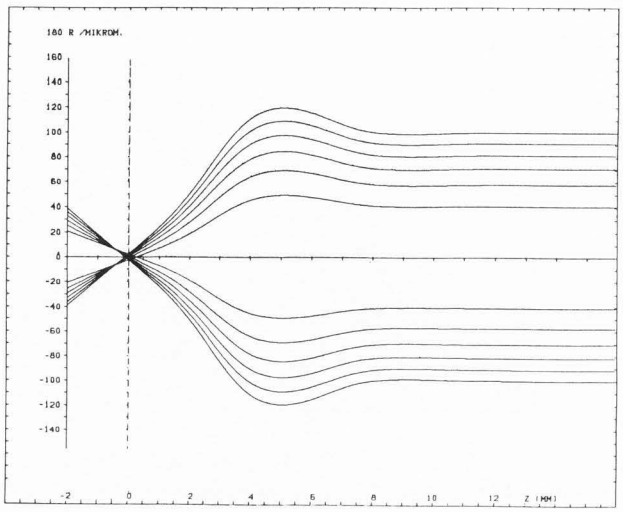

Fig. 6: Focusing of the primary beam, case of opposite charge polarity

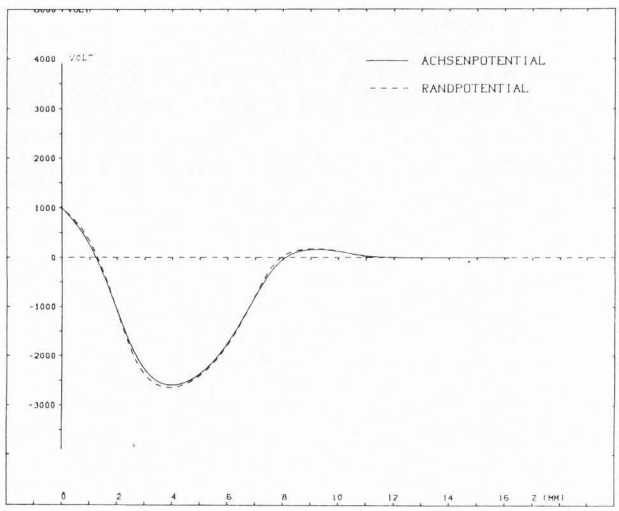

Fig. 5: Axial potential distribution, case of opposite charge polarity of primary and secondary particles

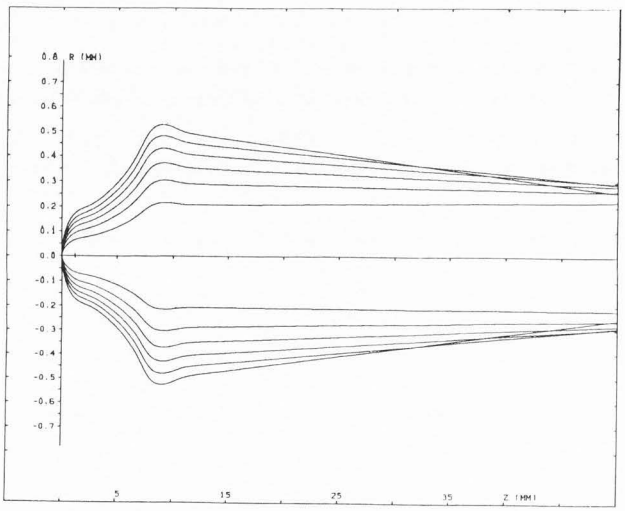

Fig. 7: Focusing of the secondary beam, case of opposite charge polarity

Figures 4 to 10 are computer plots: Figure 4 shows the geometric configuration of the electrodes generating the main field above the sample, as used for the computation.

Figure 5 shows the axial potential distribution as a result of applying certain potentials to the electrodes such that the primary beam is focused and secondaries of opposite charge polarity leave as an essentially parallel beam. The dashed curve is the potential just off the axis.

Figure 6 shows the focusing of the primary beam entering as a parallel pencil with an energy of 3.3 keV. The lens acts essentially in a decel-accel mode. Figure 7 shows the collection and focusing of the secondaries leaving the surface into the half-space with an initial energy of 5 eV. The energy of the secondary beam after leaving the field is 1 keV. Note that the axial scale is very different from that in the other plots.

Figure 8 shows an axial potential distribution which focuses the primary beam with the same entry energy of 3.3 keV in an accel-decel mode for the case of equal charge polarity particles. Figure 9 shows the focusing of the primary beam in this case. Figure 10 shows the collection and focusing of the secondaries (initial energy 5 eV) in this case. A crossover is formed right after the field. The then diverging beam is made essentially parallel by the einzel lens shown in Fig. 3 placed above the main field. The effect of this einzel lens on the primary beam is very weak, because of its higher energy, and can be corrected with the main field.

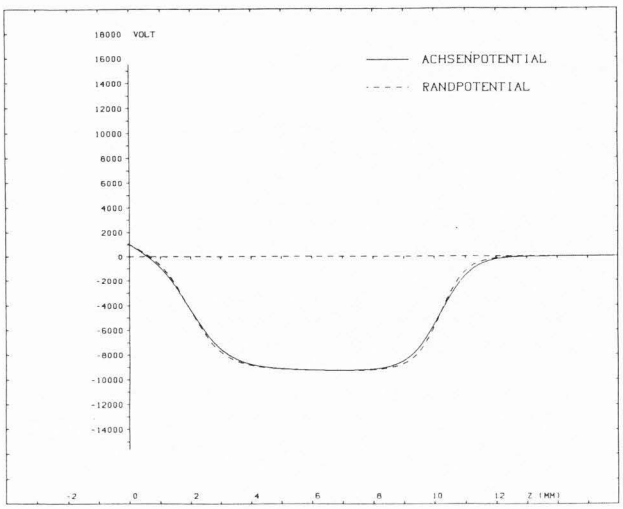

Fig. 8: Axial potential distribution, case of equal charge polarity of primary and secondary particles

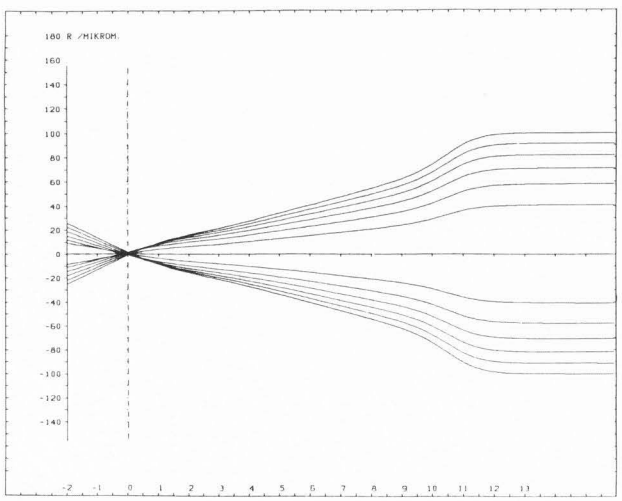

Fig. 9: Focusing of the primary beam, case of equal charge polarity

These are not the only solutions possible. An important parameter is the choice of the ratio of the energy of the primary beam entering to that of the secondary beam leaving. In the cases shown above this ratio is 3.3. The potentials applied to the electrodes scale linearly with the primary beam energy.

The plots of Figs. 6 and 9 show rather large spherical image aberrations. We have reason to believe that the program we used does not correctly yield the aberrations. In any case, in order to obtain submicron spot diameters, the diameter of the beam entering the lens can be sufficiently limited to achieve this.

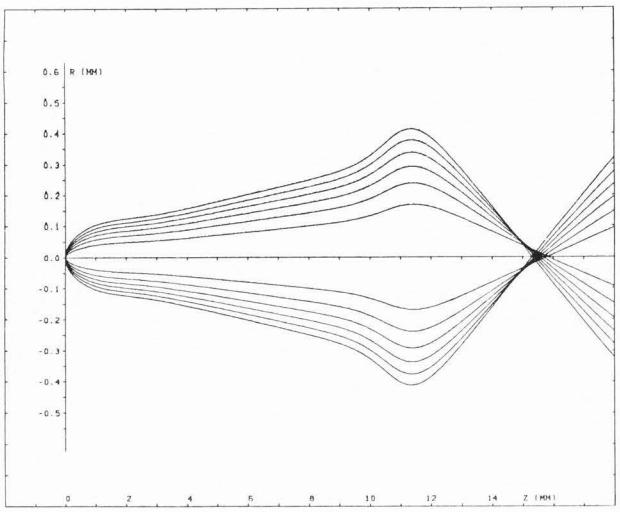

Fig. 10: Focusing of the secondary beam, case of equal charge polarity

Conclusions

The lens described above focuses the primary beam with a focal length of 5 mm in the decel-accel mode, and with a focal length of 8 mm in the accel-decel mode. These short focal lengths facilitate the achievement of very small beam probes with relatively high currents. In SIMS or SIM applications, the charged secondaries are extracted with high efficiency and formed into an essentially parallel beam for transfer into a mass spectrometer or some other detector. Scanning is best performed by double predeflection, so that the pivot point lies within the lens.

References

1. Bentz BL, Liebl H.(1982). Description and applications of a new design Cs^+ ion source on the COALA ion microprobe for negative ion SIMS, in: Secondary Ion Mass Spectrometry SIMS III, A. Benninghoven, J. Giber, J. László, M. Riedel, HW. Werner (eds.), Springer-Verlag Berlin-Heidelberg-New York, 30-37.
2. Davisson CJ, Calbick CJ (1932). Electron lenses. Phys.Rev. 42, 580.
3. Liebl H.(1972). A coaxial combined electrostatic objective and anode lens for microprobe mass analysers. Vacuum 22, 619-621.
4. Liebl H.(1978). Limits of lateral resolution in ion probe microanalysis. Adv.Mass Spectrom. 7A, 751-757.
5. Liebl H.(1979). Analytical requirements of SIMS and the instrumental implications, in: Secondary Ion Mass Spectrometry SIMS II, A. Benninghoven, CA. Evans,Jr., RA. Powell, R. Shimizu, HA Storms (eds.), Springer-Verlag Berlin-Heidelberg-New York, 176-180.
6. Liebl H.(1981). Beam optics in secondary ion mass spectrometry. Nucl.Instr.Meth. 187, 143-151.

7. Liebl H. (1983). Combined electrostatic objective and emission lenses for micro-characterization of surfaces. Int. J. Mass Spectrom. Ion Phys. 46, 511-514.
8. Liebl H. (1984). High-resolution scanning ion microscopy and secondary-ion mass spectrometry: problems and solutions. Scanning Electron Microsc. 1984; II: 519-528.
9. Liebmann G. (1949). Measured properties of strong "unipotential" electron lenses. Proc. Phys. Soc. B62, 213-228.
10. Mulvey T. (1967). Electron microprobes, in: Focusing of Charged Particles, Vol. I, A. Septier (ed), Academic Press, New York and London, 469-494.

Discussion with Reviewers

R. Levi-Setti: Is there an estimate of the energy window for the secondaries that the lens will be able to accept? This is of course important for the transmission of the system.
TR. Groves: The advantage of this system depends on a high collection efficiency of secondary ions. What is the fraction of the secondary ions which are collected to form a useful signal? The secondary ions are emitted from the sample with a range of energies, and the optical system focusses these energies differently. What is the effect of this chromatic aberration?
Authors: The trajectories of Figs. 7 and 10 are computed with an initial energy of 5 eV. This start energy was chosen because the energy distribution of sputtered ions peaks typically near this value. Starting angles to the axis are 23.1, 35.3, 45.0, 54.7, 69.9 and 90.0 degrees. With this choice of start angles, the total secondary current is subdivided into six equal portions, provided the angular emission pattern follows a cosine distribution. For secondary ions with lower initial energy the beam envelope would be slimmer, and for secondary ions with higher initial energy it would be wider. Raising or lowering of the potentials applied to the electrodes proportionally has the same effect. So a beam envelope for a given initial energy contains all ions with an initial energy of up to that value plus a fraction of ions with higher initial energy which becomes increasingly smaller with increasing initial energy. The maximum envelope diameter for the cases shown in Figs. 7 and 10 is approx. 1 mm. This can easily be accommodated by the lens, which has 2.5 mm bores at its neck (Fig. 4). In this case, the transmission through the lens could be up to 50 %, depending on the energy distribution of the sputtered ions /4/. How much of this can eventually be utilized as SIMS signal depends on the transfer optics and the acceptance of the mass spectrometer.

The effect of the chromatic aberration of the lens is small because for the range of initial energies fully transmitted the relative energy spread is small ($\lesssim$ 1/200).

R. Levi-Setti: Are there problems with an off axis incident beam? What restriction will there be on the size of the scanned area?
Authors: The deflection unit, situated above the concave mirror (Fig. 3), will be driven with d.c. voltages, causing the primary beam to enter the lens on axis in the absence of scanning. Superimposed on these d.c. voltages will be the a.c. voltages for scanning. Since the pivot point of the beam deflection lies within the lens, the maximum deflection on the sample will be given by the lateral clearance in the deflection unit multiplied by the ratio of focal length to distance to the deflection unit. The maximum scanned area will be approx. 200x200 μm^2 in size.

R. Levi-Setti: It is stated that the separation of the incoming and outgoing beam should pose no problem since they have very different energies. Yet, the ratio of such energies is 3.3 in the example shown. This implies that the extraction potential will still affect the primary beam trajectories. Will this be tolerable?
Authors: It can be seen in Figs. 5 and 8 that the sample potential is 1000 V above ground. So the energy of the secondary beam after leaving the lens will be 1 keV plus initial energy. The primary beam arrives at the lens with an energy of 3.3 keV. In the case of Fig. 5 it will hit the sample with an energy of 4.3 keV, and in the case of Fig. 8 with an energy of 2.3 keV. The primary beam trajectories are computed for this situation.

The field deflecting the secondary beam away from the axis (Fig. 3), of course, deflects the primary beam, too. This is not shown in Fig. 3, but will be compensated by appropriate pre-deflection (see above).

T. Mulvey: The plots of Figs. 6 and 9 show unbelievably large values of spherical aberration coefficient compared with the focal length. Could you quote the values of spherical aberration coefficients that you deduce from these plots and also what percentage error is likely with this method?
Authors: Two facts led us to believe that the program we used does not correctly yield the aberrations. One is the large values of the aberrations evident in Figs. 6 and 9. The aberration coefficient C_S, which can be deduced from Fig. 6, turns out to be almost 100 f, while one would expect 10 f at the most. The other fact is that, contrary to all experience, the focal length increases with the distance of the trajectories from the axis. This is all the more puzzling since the spherical aberrations of the secondary beams (Figs. 7 and 10) do show the expected behaviour. This is a highly unsatisfactory situation, indeed, and we are still working to clarify the problem.